Article

Not peer-reviewed version

Synthesis of Novel Fe-CNs-P/S Carbon Materials for Sustainable Water Treatment: Activation of Persulfate for Efficient TC Degradation

Huali Zhang , Kanghui Zhang , Qin Liu , Tongshan Shi *, Jiaheng Cui , Jinxiu Li

Posted Date: 12 September 2024

doi: 10.20944/preprints202409.0934.v1

Keywords: Sustainable Water Treatment; NH2-MIL-101 (Fe); Carbon materials; Doping; Tetracycline (TC); Persulfate activation

Article

Synthesis of Novel Fe-CNs-P/S Carbon Materials for Sustainable Water Treatment: Activation of Persulfate for Efficient TC Degradation

Huali Zhang [1], Kanghui Zhang [1], Qin Liu [1], Tongshan Shi [2,3,*], Jiaheng Cui [1] and Jinxiu Li [1]

[1] School of Chemistry and Environmental Engineering, Wuhan Institute of Technology, Wuhan, China
[2] State Key Laboratory of Efficient Utilization of Medium and Low Grade Phosphate Rock and Its Associated Resources. Guiyang 550014, China
[3] Wengfu (Group) Co., Ltd., Guiyang 550001, China
* Correspondence: sts0224995@126.com; Tel.: +86 15086160590

Abstract: This study presents a novel Fe-CNs-P/S carbon composite material, synthesized by doping elements P and S into NH_2-MIL-101 (Fe) using carbonization method. The material's application in sustainable water treatment was evaluated, focusing on its effectiveness in activating persulfate for pollutant degradation. The research thoroughly investigates the synthesis process, structural characteristics, and performance in degrading pollutants. Results indicate that Fe-CNs-P/S-5 with 50% P and S co-doping is higher than that of other samples, where the degradation rate of TC in 30min is as high as 98.11% under the optimum conditions, that is temperature at 25 ℃, 0.05 g/L of catalyst concentration, and 0.2 g/L of PMS concentration. The composite material demonstrates robust versatility and stability, maintaining high degradation efficiency across multiple organic pollutants, with no significant reduction in catalytic performance after four cycles. Furthermore, the free radical quenching experiments displays that the singlet oxygen $^1O_2$ is the main active species. It is demonstrated that the doping of P and S play a role in the enhancement of PMS activation over the Fe-CNs-P/S catalyst. This material demonstrates remarkable efficacy in treating a range of organic contaminants and exhibits excellent reusability, presenting a promising approach for enhancing sustainability in water treatment applications.

Keywords: sustainable water treatment; NH_2-MIL-101 (Fe); carbon materials; doping; tetracycline (TC); persulfate activation

1. Introduction

With the progress of economy and the development of science and technology, more and more organic pollutants produced by printing and dyeing, chemical industry, medicine and other industries are discharged into water, and the problem of organic pollution in water environment is becoming more and more serious [1–3]. TC is a tetracycline antibiotic with the molecular formula $C_{22}H_{24}N_2O_8 \cdot HCl$, which is widely used in livestock and poultry breeding and aquaculture industry. Its persistence in wastewater and soil contributes to the development of antibiotic resistance in aquatic environments and soils, posing significant risks to aquatic organisms and human health, and disrupting ecosystem balance [4,5]. Additionally, the non-degradability of antibiotics complicates their complete removal through conventional treatment methods, thereby exacerbating environmental pollution. This issue not only degrades water and soil quality directly but also impedes progress towards global Sustainable Development Goals related to clean water, healthy ecosystems, and human health. Consequently, identifying effective and eco-friendly strategies for the degradation of such organic pollutants is crucial for advancing sustainable development [6].

 doi:10.20944/preprints202409.0934.v1

Advanced oxidation technology (AOPs) has the advantages of strong oxidation ability, high free radical activity and mild reaction [7], which can make up for the poor ability of traditional biochemical methods to treat some wastewater, so it has great advantages in the treatment of highly toxic and refractory wastewater such as printing and dyeing, pesticides, pharmaceutical wastewater and landfill leachate. The types of AOPs mainly include ozonation technology, photocatalysis technology, Fenton/Fenton-like technology and so on [8,9]. Among them, persulfate activation method has attracted much attention because of its wide range of adaptation, strong anti-interference ability and strong oxidation ability.

Persulfate generally includes persulfate and peroxysulphate, among which persulfate (PDS, $S_2O_8^{2-}$) and persulfate (PMS, HSO_5^-) are the main sources of sulfate radical production [10,11]. Compared to PDS, PMS has a shorter bond length (1.46 Å) and therefore a higher O–O bond energy. The bond energy of PMS is approximately 140 kJ/mol (bond energy of PDS) and 213.3 kJ/mol (bond energy of H_2O_2) [12–14]. In addition, PMS is more easily activated due to its asymmetric molecular structure and low dissociation energy [15]. Persulfate has stable properties and weak ability to degrade organic pollutants at room temperature. It can be activated by photoactivation, zero-valent iron activation, thermal activation, microwave activation, electrochemical reduction and other methods to produce sulfate radical with stronger oxidation ($SO_4^{\cdot-}$), which can effectively degrade organic matter [16,17]. Due to the characteristics of large surface area, high porosity and good conductivity, carbon materials can be used as both adsorbent and catalyst, and are widely used in activating persulfate to degrade organic matter. Studies have shown that because the surface of carbon material is inert, its electron transport efficiency and adsorption capacity for pollutants will be affected. Therefore, the modification of carbon materials has become a current research hotspot. The commonly used modification methods are nitrogen doping, sulfur doping and metal oxide doping. After modification, the oxygen-containing functional group on the surface may be the catalytic activity center [12].

Metal-organic framework material (MOFs) is a new type of porous material with periodic network structure, which is obtained by self-assembly of metal ions and organic ligands. It has received extensive attention because of its permanent crystal structure, high specific surface area, high porosity and rich active sites [18,19].

According to the composition, MOFs can be divided into MOFs materials, MOFs composites and MOFs derived materials, in which MOFs derived materials are defined as micro/nano materials prepared by calcination, vulcanization, phosphating and other methods using MOFs materials as precursors [20–22]. Taking advantage of the advantages of MOFs, the porous carbon nanomaterials derived from MOFs can be prepared based on it, which can greatly enhance the water stability of the materials [23]. At the same time, the introduction of metal elements can increase the active sites of MOFs carbon materials and improve the physical and chemical properties of the materials [24,25]. The metal carbon materials derived from MOFs have many applications in advanced oxidation. According to the previous research, doping P, S, N and other heteroatoms in carbon materials can improve the catalytic activity of PMS/PDS for the removal of organic pollutants, because these heteroatoms can introduce more active sites, they enhance electron transfer [26,27]. Moreover, significant synergies may occur between the components of these heteroatomic carbon materials to enhance activation [28,29].

In this paper, a novel and highly efficient heterogeneous persulfate system is designed by developing carbon materials derived from NH2-MIL-101(Fe). This approach offers a sustainable technological solution for addressing organic pollutant contamination in water. NH_2-MIL-101(Fe), a metal-organic framework (MOF) material, was used as the base, into which a polymer was introduced. A one-step carbonization method was employed to prepare the P, S-doped Fe-CNs-P/S composite material. After modification, this material effectively catalyzes the activation of persulfate, leading to the degradation of organic pollutants. The doped materials provided stable P and S sources for catalyst [30]. The synthesized materials were characterized, and then their properties were evaluated by organic pollutant degradation experiments. And explore the influence of different factors on the degradation of TC by Fe-CNs-P/S activated PMS, verify the stability of the catalyst, and

 doi:10.20944/preprints202409.0934.v1

explore the possible degradation mechanism through free radical capture experiment and degraded XPS. The innovation of this research is the development of a highly catalytic and renewable material that degrades pollutants while reducing the secondary pollution problems caused by traditional treatment methods.

2. Materials and Methods

2.1. Materials

Ferric chloride hexahydrate ($FeCl_3$ $6H_2O$), N-dimethylformamide (DMF), hexachlorocyclotriphosphazene, 4-sulfonyldiphenol, triethylamine, acetone, furfuryl alcohol, anhydrous ethanol, anhydrous methanol was obtained from Sinopharm Group Chemical reagent Co., Ltd., China. 2-aminoterephthalic acid (NH_2-H_2BDC), tert-butanol, trichloromethane, potassium peroxomonosulfate was procured from Shanghai Aladdin Biochemical Technology Co., Ltd., China. tetracycline hydrochloride was procured from Beijing Biosharp Biotechnology Co., Ltd., China. The purity of all the chemical reagents were analytical grade, and water used in the experiment is deionized water.

2.2. Preparation of NH_2-MIL-101 (Fe)

Add 15 mL DMF to the bladder, dissolve 224.6 mg NH_2-H_2BDC and 675 mg $FeCl_3$·$6H_2O$ in DMF, and completely dissolve the above solids by ultrasound. Then the solution was transferred to an autoclave, the temperature was raised to 110 ℃, and maintained for 24 hours. After cooling to room temperature, the solution was put into a centrifuge. After centrifugation at 8000 rpm and time 10 min, the brown-black powder was obtained. The brown-black powder was soaked in DMF for 14 hours, filtered and then soaked in ethanol for 24 hours, and finally dried in a vacuum oven to obtain NH_2-MIL-101 (Fe).

2.3. Preparation of NH_2-MIL-101 (Fe) @ PZS

A certain quality of NH_2-MIL-101 (Fe) dissolved in 80 mL methanol was defined as X solution, while a certain quality of hexachlorocyclotriphosphazene and 4-4-sulfonyldiphenol dissolved in 20 mL methanol were defined as Y solution. X and Y were mixed, named PZS, 5 min, then added 1 mL triethylamine, stirred for 18 h, washed three times with methanol, dried in an oven at 60 ℃, and calcined in a tubular furnace at 700 ℃. Finally, NH_2-MIL-101 (Fe) @ PZS was obtained after washing and drying with water and alcohol.

The specific preparation process of NH_2-MIL-101 (Fe) @ PZS is shown in Figure 1.

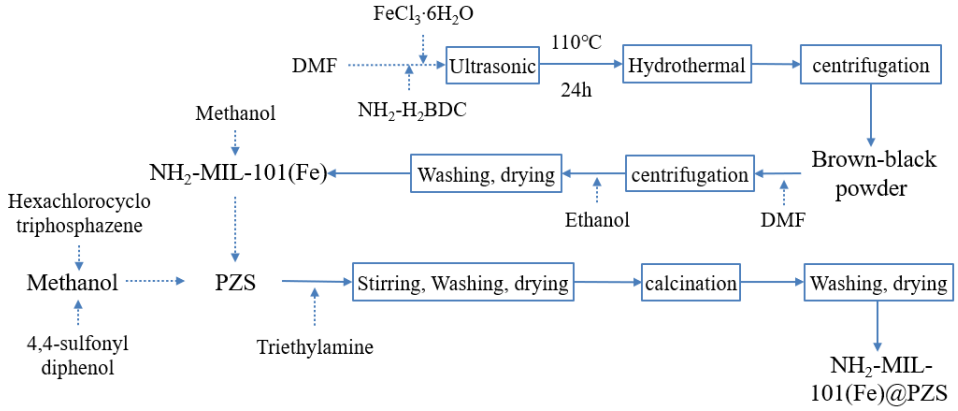

Figure 1. The flowchart of the synthesis of Fe-CNs-P/S.

2.4. Preparation of Fe-CNs-P/S

 doi:10.20944/preprints202409.0934.v1

NH_2-MIL-101 (Fe) @ PZS was put into a tube furnace, heated to 700 ℃ at a rate of 5 ℃/min under the protection of Ar atmosphere, maintained for 3 hours, then cooled to normal temperature. After washing with water and alcohol for three times, the final product Fe-CNs-P/S was obtained by drying moisture in a vacuum drying oven.

Under the same other preparation conditions, the degradation rates of Fe-CNs-P/S prepared with different ratios of P to S, NH_2-MIL-101 (Fe), hexachlorocyclotriphosphazene and 4maginyl-4-sulfonyldiphenol were studied respectively. All the experimental dosage and definition names are shown in Table 1. The final product was added to the TC solution of 20 mg/L to degrade 30 min, and the best degrader was selected according to the degradation rate, which was used in the experiment of influencing factors of TC degradation.

Table 1. List of chemical regents used in the experiments.

P/S Doping amount	NH_2-MIL-101(Fe)	Hexachlorocyclotriphosphazene	4,4-sulfonyl diphenol	Final product name
30%	0.6825 g	0.09 g	0.2025 g	Fe-CNs-P/S-3
40%	0.585 g	0.12 g	0.27 g	Fe-CNs-P/S-4
50%	0.4875 g	0.15 g	0.3375 g	Fe-CNs-P/S-5
60%	0.39 g	0.18 g	0.405 g	Fe-CNs-P/S-6
70%	0.2925 g	0.21 g	0.4725 g	Fe-CNs-P/S-7

2.5. Material Characterization

A Fourier transform infrared spectrometer (FTIR, Nicolet 6700, Thermo Fischel, USA) was used to characterize the functional groups of the samples in the wavelength range of 400–4000 cm^{-1}.

A scanning electron microscope (SEM, TalOs F200X, Thermo Fischel, USA) was used to observe the surface micromorphology of the samples, which were sprayed with gold at an acceleration voltage of 20 kV.

An X-ray diffractometer (XRD, D/MAX-RB, Japan) was used to analyze the aggregated structure of the samples in the 2θ scanning range of 10°–80° with a scanning speed of 0.02°. The test was operated with Cu-Kα radiation at a voltage of 40 kV and a current of 50 mA.

An X-ray photoelectron spectroscopy (XPS, ESCALAB Ⅱ, Thermo Fischel, USA) was used to analyze chemical compositions and metal valence states, with the binding energy of C1s (284.8 eV) as the control standard and Al Ka as the X-ray source.

A specific surface area porosity analyzer (BET, ASAP2020 HD88, Mack Instruments, USA) was used to measure the specific surface area and aperture. The material was heat treated at 120℃ under nitrogen atmosphere for 2h, and then the sample was subjected to nitrogen adsorption and desorption under liquid nitrogen environment to measure the specific surface area and aperture.

A Raman spectrometer (Raman, Renishaw 2000, China) was used to analyze the surface molecular structure, with a spectral scanning range of 800–3000 cm^{-1}.

2.6. Degradation of TC

The 5 mg catalyst was dissolved in the TC solution of 100 mL 20 mg/L, the 30 min was stirred by magnetic force, and remove 3mL from it for centrifugation. The supernatant was placed at the ultraviolet spectrophotometer 356 nm to determine the absorbance.

20 mg PMS was added to TC solution, sampled at the same time interval, and its absorbance was measured after centrifugation. The degradation rate was determined as follows:

$$\eta = (C_0 - C_t)/C_0 \times 100\%, \quad (1)$$

where η is the degradation rate; C_0 is the initial concentration; C_t is the concentration at t time.

 doi:10.20944/preprints202409.0934.v1

In the experiment of studying the effect of initial pH on degradation, 1 mol/L NaOH and 1 mol/L HNO_3 were used to adjust pH value. In the catalyst cycle experiment, the catalyst was centrifuged, washed with water, washed with alcohol and dried.

3. Results

3.1. Characterization of Materials

3.1.1. XRD Analysis

Firstly, the crystal structures of all samples were characterized by XRD. Figure 2 shows the XRD patterns of Fe-CNs-P/S-3, Fe-CNs-P/S-4, Fe-CNs-P/S-5, Fe-CNs-P/S-6 and Fe-CNs-P/S-7. In the Fe-CNs-P/S-5, in Figure 2a, the broad peak detected at 22.6 is caused by the amorphous polymer PZS. The diffraction peaks of Fe-CNs-P/S-5 are 2θ = 28.8°, 30.1°, 35.5°, 39.9°, 41.0°, 44.5°, 50.7°, 52.1°, 53.1°, corresponding to the crystal planes of FeP_4, respectively. The peak diffraction spectrum of Fe-CNs-P/S-5 is 35.2°, 39.8°, 43.7°, 44.6°and 64.9°, corresponding to the crystal planes of Fe_3C, respectively, indicating that FeP_4 and Fe_3C may exist in Fe-CNs-P/S-5 [30]. According to Figure 2b, the peaks of Fe-CNs-P/S-3, Fe-CNs-P/S-4, Fe-CNs-P/S-5 and Fe-CNs-P/S-6 are basically the same, while different Fe-CNs-P/S-7 lacks peak patterns. This phenomenon may be due to the high content of PZS in Fe-CNs-P/S-7, the low content of NH_2-MIL-101 (Fe), and the coating of PZS on the surface of MOFs. So that the material is not fully carbonized.

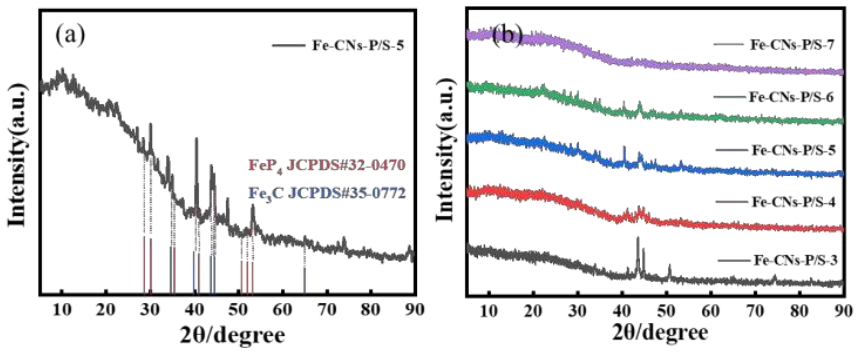

Figure 2. (a) XRD pattern of the Fe-CNs-P/S-5, (b) XRD patterns of the prepared Fe-CNs-P/S-3, Fe-CNs-P/S-4, Fe-CNs-P/S-5, Fe-CNs-P/S-6 and Fe-CNs-P/S-7.

3.1.2. SEM Analysis

The morphology of Fe-CNs-P/S-5 was characterized by SEM. Figure. 3 shows the SEM pattern. According to the graph shown in Figure 3a, it is not difficult to see that there are smooth small bulk and irregular solid structure on the surface of Fe-CNs-P/S-5 sample. In Figure 3b and c, irregular solids can be observed near the smooth small bulk, so the small bulk may be an incomplete MOFs structure protected by PZS, while the irregular solid may be a carbon material formed by PZS calcination. Figure 3b also shows that the irregular solid surface is an uneven spongy structure loaded with pellets. The surface elements of Fe-CNs-P/S-5 were characterized by EDS. Figure. 3d shows the distribution of elements C, O, N, P, S and Fe in Fe-CNs-P/S-5. All the above elements exist and are distributed uniformly, so it can be inferred that P and S have been successfully doped into carbon materials.

 doi:10.20944/preprints202409.0934.v1

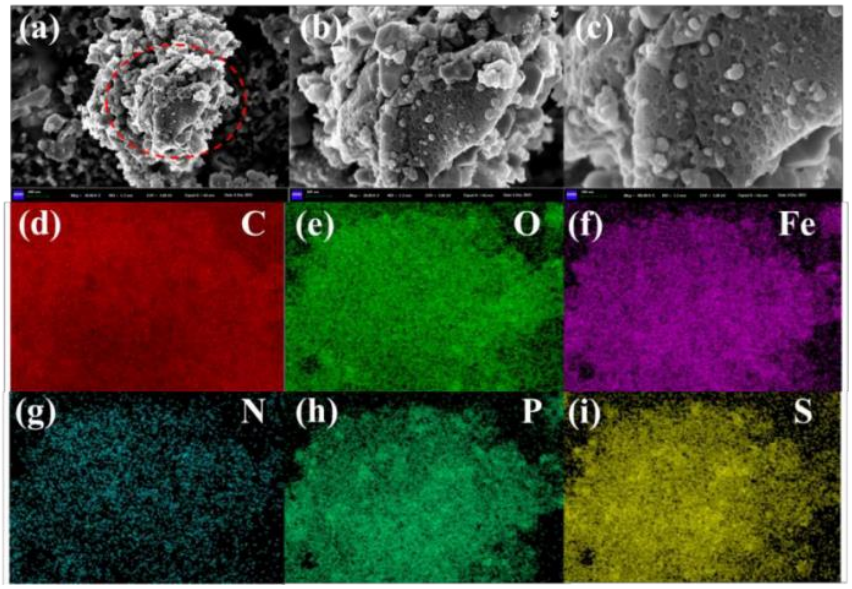

Figure 3. (a-c) SEM images of Fe-CNs-P/S-5, (d-i) elemental mapping of the prepared Fe-CNs-P/S-5 sample.

3.1.3. TEM Analysis

The morphology and structure of Fe-CNs-P/S-5 were further analyzed by TEM characterization. In Figure 4a,b, it is shown that small black particles attributed to the metallic iron can be observed in the dark gray carbon layer. From Figure 4c and d enlarged to 200 nm, it can be seen that the dark gray carbon layer is fragmented and accumulated, which may be formed by PZS carbonization. According to Figure 4e,f, we can see that the dark gray carbon layer has an irregular structure, which is basically consistent with the previous SEM image.

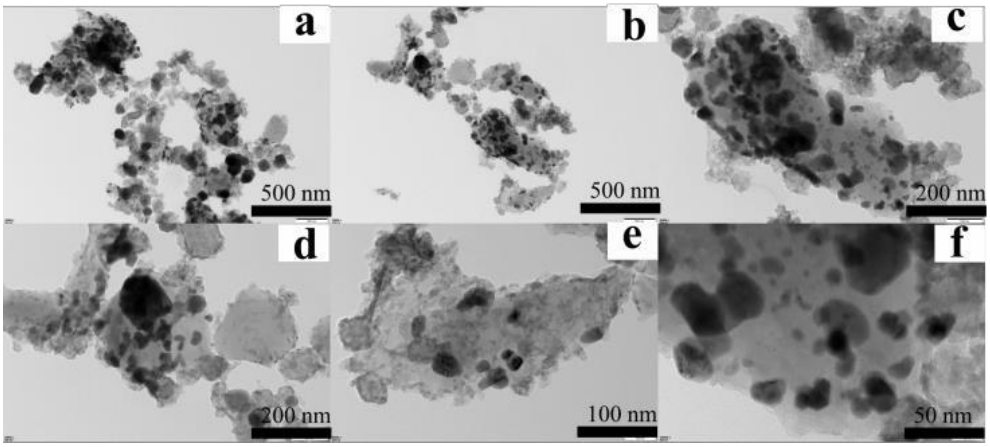

Figure 4. (a-f) TEM images of Fe-CNs-P/S-5 with different magnifications.

3.1.4. XPS Analysis

The type, valence and bonding of elements in the Fe-CNs-P/S-5 sample were further analyzed by XPS. Figure 5 shows the XPS map. According to Figure 5a, Fe-CNs-P/S-5 contains C, O, N, P, S and Fe elements. The order of content is C > O > Fe > N > S > P, S, C content is the highest, P, S content is lower. As the shown in Figure 5b, the C 1s energy spectrum corrected by 284.8eV, and the peak of C–C bond at 284.8eV and the peak of C–N bond is located at 285.6 eV. The characteristic peaks of Fe^{2+} (710.5 and 723.8 eV) and Fe^{3+} (712.8 and 725.8 eV) are shown in the Fe 2p energy spectrum (Figure 5c). The two peaks centered on 132.9 and 133.7 eV in the P 2p energy spectrum (Figure 5d) correspond to the P–C bond and P–O bond, respectively. The S 2p energy spectrum (Figure 5e) shows that the

 doi:10.20944/preprints202409.0934.v1

three peaks at 163.5, 164.6 and 168.5 eV correspond to S $2p_{1/2}$, S $2p_{3/2}$ and oxidized S [31], respectively. Figure 5d,e illustrate the deconvolution results of P 2p and S 2p, which proves that P and S elements are doped successfully.

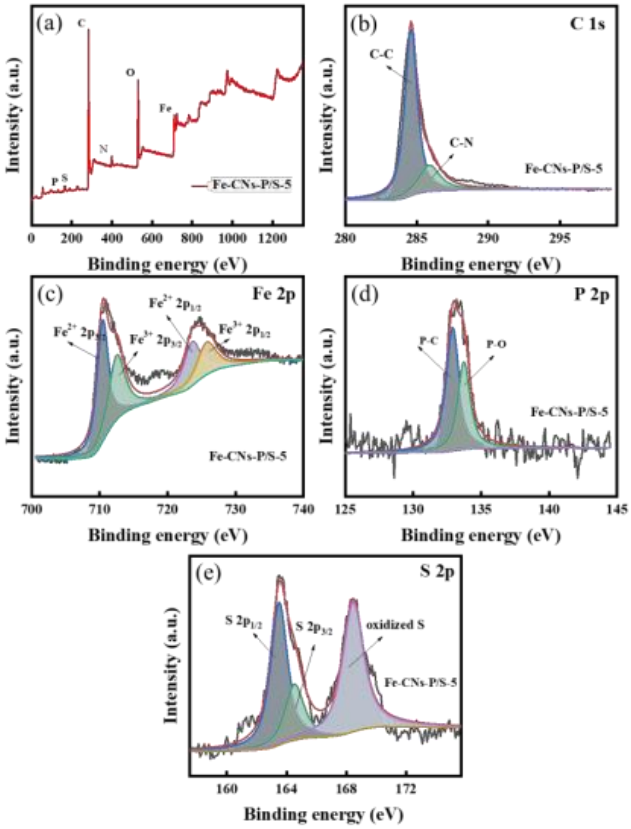

Figure 5. XPS spectra of the Fe-CNs-P/S-5 sample: (a) full spectrum, (b) C 1s, (c) Fe 2p , (d) P 2p and (e) S 2p.

3.1.5. FTIR Analysis

Figure 6 is the infrared spectrum of Fe-CNs-P/S-5, which shows that 560 cm^{-1} and 1070 cm^{-1} correspond to the stretching peak of Fe–O and the strong absorption vibration peak of O=S=O, respectively. It is speculated that 1230 cm^{-1} may be ascribed to the stretching vibration of P–H, indicating that P and S are doped successfully. Meanwhile, the peak at 1560 cm^{-1} corresponds to the stretching vibration peak of benzene ring, indicating that the benzene ring on the MOFs has not been burned. Another weak peak centered at 2800 cm^{-1} corresponds to the stretching vibration peak of C–H, and 3190 cm^{-1} corresponds to the stretching vibration peak of N–H.

 doi:10.20944/preprints202409.0934.v1

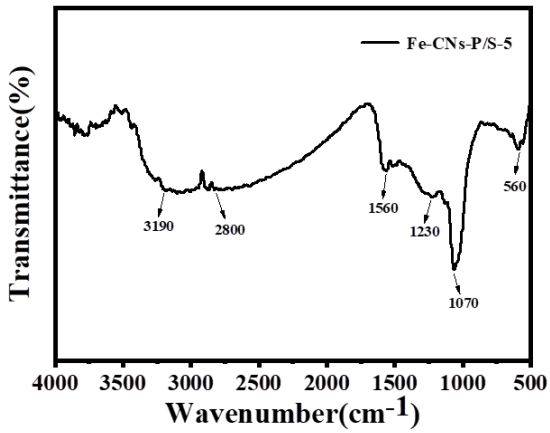

Figure 6. FTIR spectrum of the Fe-CNs-P/S-5 sample.

3.1.6. BET Analysis

Figure 7 shows the N_2 adsorption/desorption isotherm of Fe-CNs-P/S-5. It is observed that the specific surface area, average pore size and pore volume of Fe-CNs-P/S-5 are 203.8 m^2/g, g 6.15 nm and 0.13 cm^2/g, respectively. According to IUPAC classification, the sample shows a typical IV isotherm and hysteresis curve, which can be classified as H4 type. The material shows a sharp increase in adsorption capacity under relatively low pressure conditions, which verifies the existence of micropores. The illustration in Figure 7 shows the lag characteristic of the parallel adsorption/desorption curve of capillary condensation, showing the pore size and pore volume distribution. The pore size of Fe-CNs-P/S-5 is mainly distributed at about 3 nm.

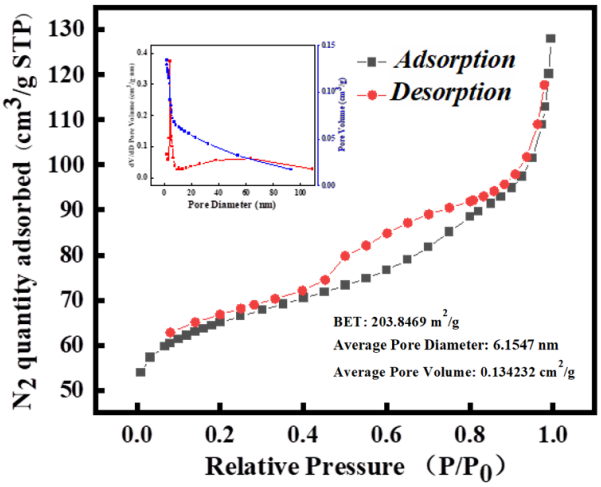

Figure 7. N_2 adsorption/desorption isotherm of Fe-CNs-P/S-5.

3.1.7. Raman Analysis

Figure 8 shows the Raman spectra of Fe-CNs-P/S-3, Fe-CNs-P/S-4, Fe-CNs-P/S-5, Fe-CNs-P/S-6 and Fe-CNs-P/S-7. The I_D/I_G of the five materials are 1.98, 1.59, 2.2, 1.14 and 1.03, respectively. The reason is that the doping of P and S will promote the formation of defects, change the charge distribution of carbon network and destroy its inertia. Thus, the defect degree of the material is high [32]. The defect degree of Fe-CNs-P/S-5 is the highest, indicating that the defect degree of the material is affected by the amount of P and S doping. Generally speaking, the degree of defects seriously affects the adsorption of PMS and the transfer of π-free electrons from sp^2 hybrid carbon network to PMS [33]. The structural defects can be used as active sites for the formation of active components to

 doi:10.20944/preprints202409.0934.v1

promote redox catalysis [34]. When the doping amount of P and S increases, the I_D/I_G value decreases continuously, which may be due to decreasing of active sites after the doping amount.

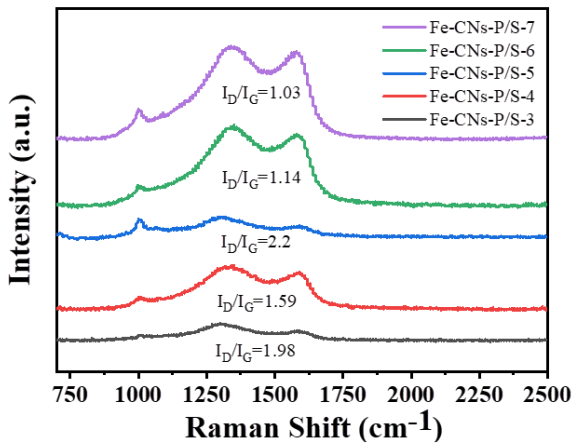

Figure 8. Raman spectra of the Fe-CNs-P/S-3, Fe-CNs-P/S-4, Fe-CNs-P/S-5, Fe-CNs-P/S-6 and Fe-CNs-P/S-7.

3.2. Degradation of TC

3.2.1. Effect of P/S Doping Amount

Because doping other atoms can affect the degradation rate of TC via catalyst activated persulfate, activation degradation performance of TC over the Fe-CNs-P/S by different amount of P and S doping in order to determine the highest degradation rate of P and S doping have been investigated. Figure 9a depicts the effect of different amounts of P and S doping on the degradation of TC. The degradation rates of TC over the Fe-CNs-P/S-3, Fe-CNs-P/S-4, Fe-CNs-P/S-5, Fe-CNs-P/S-6 and Fe-CNs-P/S-7 are 87.73%, 91.3%, 98.11%, 78.67% and 51.4%, respectively. When the ratio reaches 50%, the degradation rate is the highest However, when the amount of doping increases, the degradation rate decreases because too much doping will lead to decreasing of active sites [33]. Figure 9b shows that the degradation rates of TC by Fe-CNs-P/S-5 and PMS in 30 min are 27.4% and 40.54%, respectively. The data show that when Fe-CNs-P/S-5 and PMS degrade TC alone, the degradation ability is not prominent. At the same time, it was found that the TC degradation rate of Fe-CNs-P/S-5 activated PMS was significantly higher than that of activated PDS, and it was concluded that Fe-CNs-P/S-5/PMS system had the best performance of TC degradation.

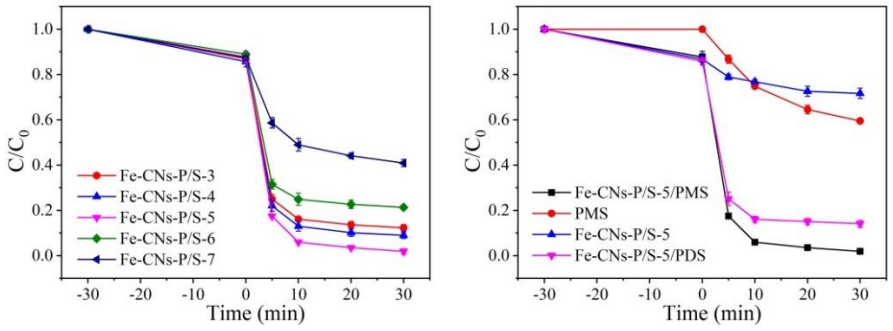

Figure 9. (a) Degradation efficiency of TC by Fe-CNs-P/S activated PMS and (b) Degradation efficiency of TC by Fe-CNs-P/S-5 activated PMS/PDS.

 doi:10.20944/preprints202409.0934.v1

3.2.2. Effect of P/S Doping Amount

Figure 10 shows effects of the amount of catalyst on the degradation of TC by Fe-CNs-P/S-5/PMS. The dosage of PMS is 0.2 g, the initial concentration of TC is 20 mg/L, and the dosage of Fe-CNs-P/S-5 is 0.05, 0.1 and 0.2 g/L, respectively. It can be seen that when the dosage of Fe-CNs-P/S-5 is 0.05 g/L, the degradation rate of TC is 98.11%. With the increase of the amount of catalyst, the degradation rate of TC increases gradually, but the increase is not obvious. Considering the economy of the experiment, 0.05 g/L is finally selected as the best dosage for Fe-CNs-P/S-5 experiment.

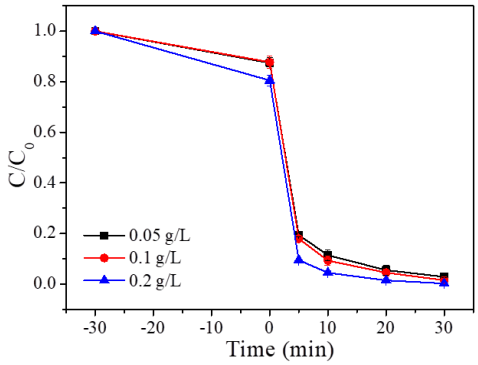

Figure 10. Effect of catalyst dosage on TC degradation by the Fe-CNs-P/S-5/PMS system.

3.2.3. Effect of P/S Doping Amount

Figure 11 shows the effect of PMS dosage on the degradation of TC by Fe-CNs-P/S-5/PMS. When the amount of catalyst is 0.05 g/L, the initial concentration of TC is 20 mg/L, the dosage of PMS is 0.1, 0.2 and 0.5 g/L, respectively. It can be seen from Figure11 that with the increase of the amount of PMS, the degradation rate of TC by Fe-CNs-P/S-5/PMS increases gradually, and the degradation rate of TC in 0.2 g/L and 0.5 g/L is 98.1% and 98.5% respectively, and the difference in degradation effect is small. It may be that the limited active sites cannot accommodate too much PMS, and further increasing the amount of PMS will lead to a decrease in the degradation rate, so 0.2 g/L is chosen as the best concentration in the experiment.

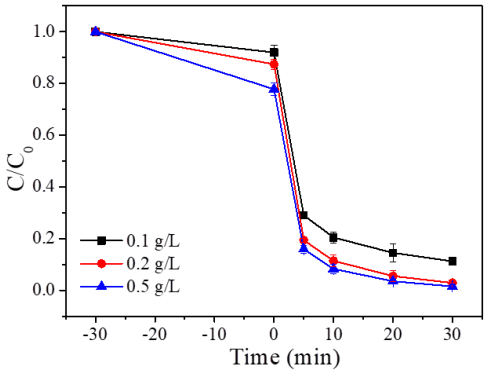

Figure 11. Effect of PMS concentration on TC degradation by the Fe-CNs-P/S-5/PMS system.

3.2.4. Effect of P/S Doping Amount

Under the experimental conditions, when the dosage of catalyst is 0.05 g/L, the dosage of PMS is 0.2 g/L. As shown in Figure 12, it can be seen that the degradation rate of TC decreases gradually with the increase of initial concentration. When the initial concentration of TC is 10 and 20 mg/L, the degradation rate of Fe-CNs-P/S-5/PMS to TC is 98.6% and 98.11%, respectively, but when the initial concentration of TC increases to 30 mg/L, the degradation rate of TC is 98.6% and 98.11%, respectively. The degradation rate decreased to 90.26%. Considering the degradation performance of Fe-CNs-P/S-5/PMS, the best initial concentration of TC was determined to be 20 mg/L.

 doi:10.20944/preprints202409.0934.v1

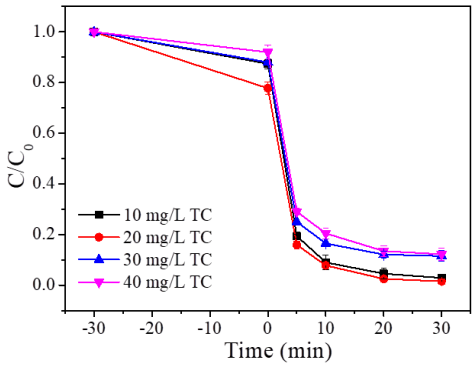

Figure 12. Effects of initial concentration on the degradation of TC.

3.2.5. Effect of Initial pH of Solution

The initial pH of the solution is also an important factor affecting the degradation of TC. As shown in Figure 13, the experimental conditions are controlled as the amount of catalyst is 0.05 g/L, the dosage of PMS is 0.2 g/L, the initial concentration of TC is 20 mg/L, the initial pH is 3.06, 5.12, 7.33, 9.11, it can be observed that the degradation rate of TC is more than 89.8%, indicating that a high TC degradation rate can be obtained between 3 and 9 [35].

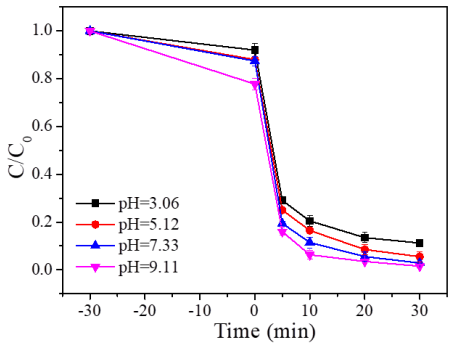

Figure 13. Effect of initial pH of solution on degradation of TC.

3.2.6. Effect of Inorganic Anions

There are some inorganic anions in natural water. In order to make the simulated wastewater closer to the actual wastewater, inorganic anions such as CO_3^{2-}, Cl^-, HPO_4^{2-}, HCO_3^- and SO_4^{2-} were added to the simulated wastewater, and the influence of each anion on the degradation of TC by Fe-CNs-PS-5/PMS was explored [36].

The experimental conditions were controlled as follows: the amount of catalyst was 0.05 g, the dosage of PMS was 0.2 g/L, and the initial concentration of TC was 20 mg/L. As shown in Figure 1a,b, when Na_2CO_3 and NaCl of 10 mM were added to the above system, it was observed that Cl^- and CO_3^{2-} had little inhibitory effect on degradation, but when the dosage increased to 50 mM, there was still no obvious inhibitory effect, indicating that Cl^- and CO_3^{2-} had little inhibitory effect on the degradation of TC [37,38]. It can be seen from Figure 14c that when Na_2HPO_4 and Na_2SO_4 of 10 mM are added to the system, the degradation rate of TC increases, and when the dosage increases to 50 mM, the degradation rate of TC increases slightly, indicating that HPO_4^{2-} and SO_4^{2-} can promote the degradation of TC. As shown in Figure 14, when the concentration of HCO_3^- is increased from 10 mM to 50 mM, the degradation rate of TC decreases gradually, which may be the fact that HCO_3^- acts as a free radical scavenger, thus reducing the catalytic performance.

Preprints.org (www.preprints.org) | NOT PEER-REVIEWED | Posted: 12 September 2024 doi:10.20944/preprints202409.0934.v1

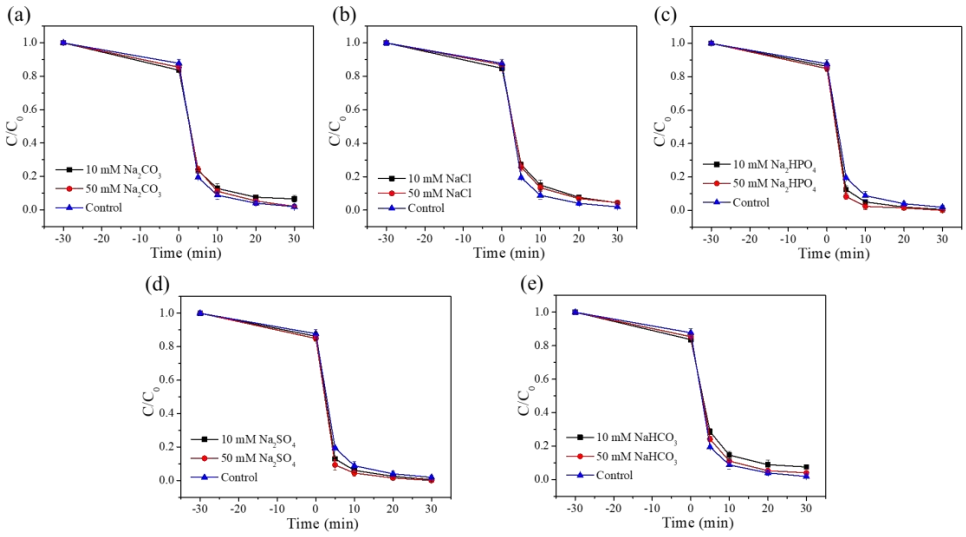

Figure 14. Effects of different anions on the degradation of TC in Fe-CNs-P/S-5/PMS system: (a) Cl^-,(b) CO_3^{2-},(c) HCO_3^-,(d) HPO_4^{2-},(e) SO_4^{2-}.

3.2.7. Cycle Efficiency

All the experimental results show that Fe-CNs-P/S-5 has good catalytic activity, and in practical application, stability is also an index to measure the quality of the catalyst. Figure 15 shows the cyclic effect of Fe-CNs-P/S-5/PMS system on the degradation of TC. The dosage of Fe-CNs-P/S-5 is 0.05 g/L, the initial concentration of PMS is 0.2 g/L, the initial concentration of TC is 20 mg/L. The data showed that the degradation rate of TC was not significantly affected after the catalyst was recycled for 4 times, and the degradation rate of each cycle was more than 88.3%. At the same time, in 20 mg/L TC solution of 100 mL, the dissolution amount of iron ion in Fe-CNs-P/S-5/PMS system is 0.071 mg/L, indicating that Fe-CNs-P/S-5 can activate PMS is the role of catalyst. Further confirmed that the Fe-CNs-P/S-5 has good water stability, iron dissolution risk is low, conducive to the sustainable use of materials in practical application.

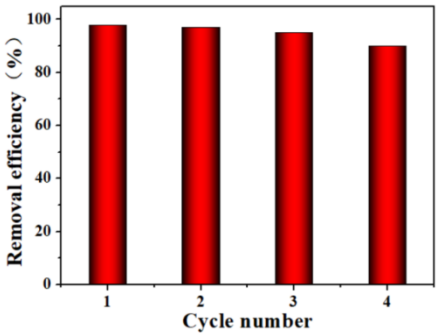

Figure 15. Recycle efficiency for TC degradation by the Fe-CNs-P/S-5/PMS system.

3.2.8. Universality

Figure 16 illustrates the degradation of different pollutants by the Fe-CNs-P/S-5/PMS system. The study investigated Acid Red G, Methyl Orange (MO), Acid Orange 7 (AO7), and Bisphenol A (BPA) at a concentration of 20 mg/L. The experimental results demonstrate that the Fe-CNs-P/S-5/PMS system exhibits a high removal efficiency for all four pollutants, achieving removal rates exceeding 90%. This indicates that the Fe-CNs-P/S-5 material has excellent universal applicability and is well-suited for complex water environments. Consequently, it can serve as an effective catalyst for the degradation of challenging wastewater in practical applications.

 doi:10.20944/preprints202409.0934.v1

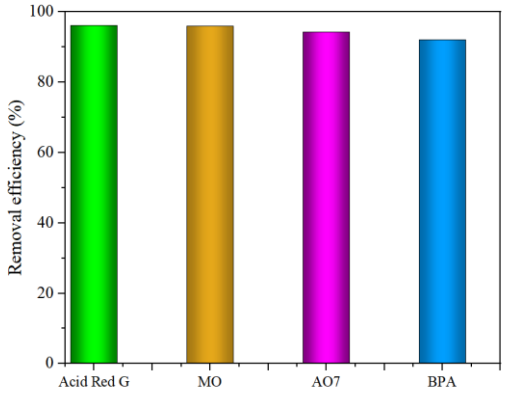

Figure 16. Degradation of different pollutants by the Fe-CNs-P/S-5/PMS system.

3.2.9. Free Radical Quenching Experiment

In order to further determine the types of active substances in Fe-CNs-P/S-5/PMS system, quenching experiments were carried out by adding scavengers with different free radicals to evaluate the role of free radicals in the degradation of TC. As shown in Figure 17, when the collectors of tert-butanol, ethanol, furfuryl alcohol and $CHCl_3$ are ·OH, $SO_4^{\cdot-}$, ($^1O_2$) and ($\cdot O_2^-$) respectively, when 10 mM of $CHCl_3$, tert-butanol and ethanol are added, the TC degradation rate is reduced by only 1%. When the radical scavengers are added and reached 100 mM, the TC degradation rate decreases by 3%-7%, indicating that Cl^-, ·OH and $SO_4^{\cdot-}$ play a small role in the system. When 10 mM furfuryl alcohol was added to the system, the degradation rate of TC decreased by 50.1%, and when it was further added to 100 mM, the degradation rate decreased by 86.3%, and its catalytic activity was almost completely inhibited, so it can be proved that $^1O_2$ plays a leading role in the system.

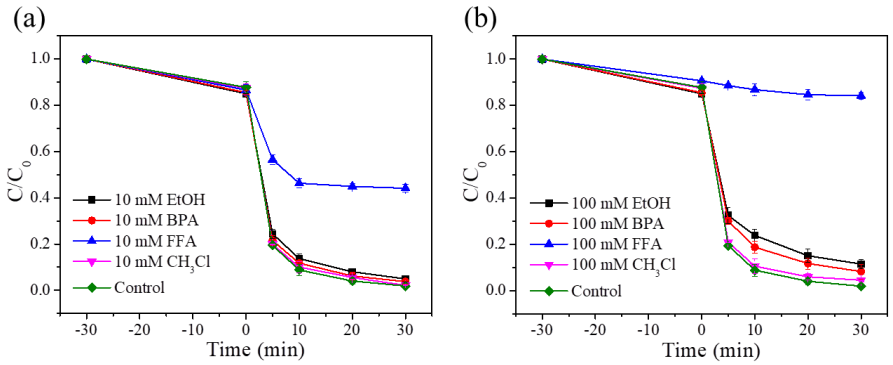

Figure 17. Effects of 10 mM different radical scavengers and (b) 100 mM different radical scavengers on the degradation of TC in the Fe-CNs-P/S-5/PMS system.

3.2.10. XPS Analysis before and after Degradation

Figure 18 shows the XPS of the catalyst before and after degradation. The C 1s spectrum is shown in Figure 18a. The image shows that there is no obvious change before and after the degradation of the catalyst, and there are peaks of C–C bond and C–N bond at 284.8 eV and 285.6 eV. The Fe 2p spectrum is shown in Figure 18b. Compared with the previous catalyst, the characteristic peaks of Fe^{2+} (710.7 and 724.0 eV) and Fe^{3+} (712.6 and 725.8 eV) shift 0.2 eV. The cyclic XPS of P 2p is shown in Figure 18c. The positions of the peaks of P–C bond and P–O bond is 133.2 and 133.9 eV, an increase of 0.2 eV. The cyclic S 2p XPS diagram is shown in Figure 18d. It can be seen that S 2p is basically unchanged at S $2p_{1/2}$ and S $2p_{3/2}$ at 163.6 and 164.6 eV, respectively, but the position of the oxidized S

 doi:10.20944/preprints202409.0934.v1

peak is shifted to 169.0 eV, and the proportion is increased from 45% to 72%, indicating that P and S play a role in catalysis.

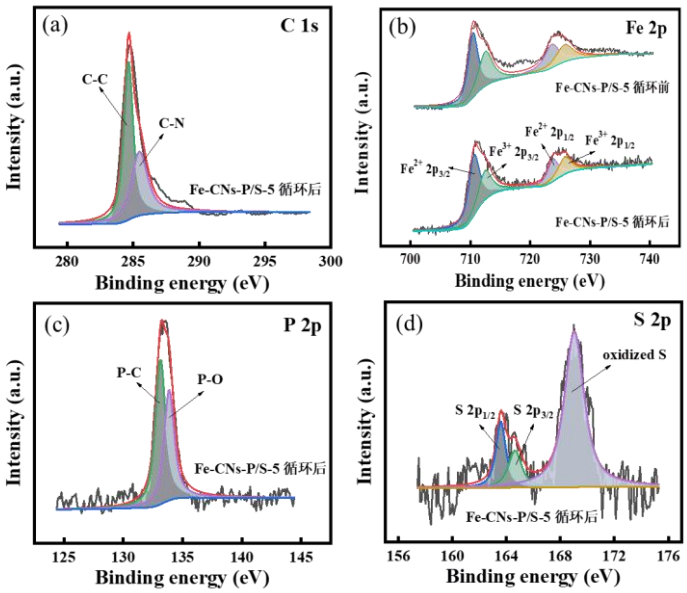

Figure 18. XPS spectra of Fe-CNs-P/S-5 after degradation (a) C 1s, (b) Fe 2p,(c) P 2p and (d) S 2p.

Based on the above image analysis, the specific mechanism of Fe-CNs-P/S-5/PMS system activating PMS to degrade TC: when the PMS whose main active component is HSO_5^- is dissolved in water, a small amount of SO_5^{2-} will be formed (Formula (2)), and then SO_5^{2-} reacts with HSO_5^- to produce a small amount of $^1O_2$ (Formula (3)) [39]. Fe^{2+} and C in Fe-CNs-P/S-5 become active sites in the catalytic process and participate in the activation of PMS to produce a large number of $SO_4^{\cdot-}$ and SO_5^{2-} (Formulas (4)–(6)) [40,41]. $SO_5^{\cdot-}$ radical not only reacts spontaneously to form $S_2O_8^{2-}$ ion and $^1O_2$ (Formula (7)), but also reacts with $SO_5^{\cdot-}$and HSO_5^- to form $^1O_2$ (FORMULA (8)) [42,43]. The resulting $^1O_2$ reacts with TC adsorbed on the surface of the catalyst to degrade organic pollutants. The specific reaction mechanism is as follows:

$$HSO_5^- \rightarrow SO_5^{2-} + H^+, \quad (2)$$

$$HSO_5^- + SO_5^{2-} \rightarrow 2SO_4^{2-} + {}^1O_2 + H^+, \quad (3)$$

$$Fe(II) + PMS(HSO_5^-) \rightarrow Fe(III) + SO_4^{\cdot-} + OH^-, \quad (4)$$

$$Fe(III) + PMS(HSO_5^-) \rightarrow Fe(II) + SO_5^{\cdot-} + H^+, \quad (5)$$

$$Carbon + PMS(HSO_5^-) \rightarrow carbon\text{-}oxidized + SO_4^{\cdot-} + OH^-, \quad (6)$$

$$SO_5^{\cdot-} + SO_5^{\cdot-} \rightarrow S_2O_8^{2-} + {}^1O_2, \quad (7)$$

$$SO_5^{\cdot-} + HSO_5^- \rightarrow HSO_4^{2-} + {}^1O_2, \quad (8)$$

4. Conclusions

In this paper, Fe-CNs-P/S was successfully prepared by solvothermal method, organic polymerization and one-step carbonization method. The phase composition, microstructure and surface characteristics of Fe-CNs-P/S were characterized by XRD, SEM, XPS and other

 doi:10.20944/preprints202409.0934.v1

characterization methods. The prepared Fe-CNs-P/S was used to activate PMS to degrade TC in the simulated wastewater, and the effects of different factors on the degradation of TC by this system were discussed. Fe-CNs-P/S-5 showed high catalytic activity in the degradation of TC in Fe-CNs-P/S/PMS system, and under the optimum conditions (Fe-CNs-P/S-5:0.05 g/L). Fe-CNs-P/S-5 can degrade 98.11% of 20 mg/L TC at 30 min, which is better than other mass ratio catalysts for TC degradation under the same conditions. Fe-CNs-P/S-5/PMS system has good catalytic performance and good stability in a wide range of pH value. Through capture experiments, it can be inferred that the main free radical in the reaction system is $^1O_2$, and the possible mechanism of TC degradation by Fe-CNs-P/S-5/PMS system is given. In conclusion, this paper provides an efficient and universal route for the treatment of organic pollutants by introducing sustainable materials based on Fe-CNs-P/S. This material has good universality and renewability, and does not produce secondary pollution in the process of use. It is expected to help reduce pollutant emissions in future large-scale industrial applications, improve resource utilization efficiency, and promote the sustainable development of environmental governance.

Acknowledgments: This work was supported by State Key Laboratory of Efficient Utilization of Medium and Low Grade Phosphate Rock and its Associated Resource[WFKF(2020)003], Wengfu(Group)Co., ltd. and Graduate Innovative Fund of Wuhan Institute of Technology[CX2023147].

Conflicts of Interest: Tongshan Shi was employed by the State Key Laboratory of Efficient Utilization of Medium and Low Grade Phosphate Rock and Its Associated Resources. The remaining authors declare that the research was conducted in the absence of any commercial or financial relationships that could be construed as a potential conflict of interest.

Funding: The authors declare that this study received funding from State Key Laboratory of Efficient Utilization of Medium and Low Grade Phosphate Rock and its Associated Resource[WFKF(2020)003] and Graduate Innovative Fund of Wuhan Institute of Technology[CX2023147]. The funder was not involved in the study design, collection, analysis, interpretation of data, the writing of this article or the decision to submit it for publication.

References

1. Hena, S.; Gutierrez, L.; Croué, J.-P. Removal of Pharmaceutical and Personal Care Products (PPCPs) from Wastewater Using Microalgae: A Review. *J. Hazard. Mater.* **2021**, *403*, 124041. https://doi.org/10.1016/j.jhazmat.2020.124041.
2. Xiang, Y.; Wu, H.; Li, L.; Ren, M.; Qie, H.; Lin, A. A Review of Distribution and Risk of Pharmaceuticals and Personal Care Products in the Aquatic Environment in China. *Ecotoxicol. Environ. Saf.* **2021**, *213*, 112044. https://doi.org/10.1016/j.ecoenv.2021.112044.
3. Yang, Z.; Cao, J.; Chen, Y.; Li, X.; Xiong, W.; Zhou, Y.; Zhou, C.; Xu, R.; Zhang, Y. Mn-Doped Zirconium Metal-Organic Framework as an Effective Adsorbent for Removal of Tetracycline and Cr(VI) from Aqueous Solution. *Microporous Mesoporous Mater.* **2019**, *277*, 277–285. https://doi.org/10.1016/j.micromeso.2018.11.014.
4. Zhu, P.; Li, Y.; Chen, F.; Luo, X.; Zhou, Y.; Qiu, Q.; Xie, T. Construction of 3D Flower-like $FeTiO_3$/MoS_2Heterostructure Photocatalyst for Degradation of Tetracycline Hydrochloride. *Journal of Alloys and Compounds* **2023**, *937*, 168425. https://doi.org/10.1016/j.jallcom.2022.168425.
5. Golrizkhatami, F.; Taghavi, L.; Nasseh, N.; Panahi, H. A. Synthesis of Novel $MnFe_2O_4$/BiOI Green Nanocomposite and Its Application to Photocatalytic Degradation of Tetracycline Hydrochloride: (LC-MS Analyses, Mechanism, Reusability, Kinetic, Radical Agents, Mineralization, Process Capability, and Purification of Actual Pharmaceutical Wastewater). *Journal of Photochemistry and Photobiology A: Chemistry* **2023**, *444*, 114989. https://doi.org/10.1016/j.jphotochem.2023.114989.
6. Van Tri, D.; Barcelo, D.; Le Luu, T. The Performances of Persulfate Activators to Degrade the Persistent Organic Pollutants in Industrial Wastewater. *Case Studies in Chemical and Environmental Engineering* **2023**, *8*, 100539. https://doi.org/10.1016/j.cscee.2023.100539.
7. Bautista, P.; Mohedano, A. F.; Casas, J. A.; Zazo, J. A.; Rodriguez, J. J. An Overview of the Application of Fenton Oxidation to Industrial Wastewaters Treatment. *Journal of Chemical Technology & Biotechnology* **2008**, *83* (10), 1323–1338. https://doi.org/10.1002/jctb.1988.
8. Wang, X.; He, L.; Zhou, Y.; Wang, N.; Zhu, L.; Yan, J.; Ding, D.; Zhu, W.; Zuo, X.; Wang, J.; Wu, X. Deep Mineralization of Bisphenol A via Cu–Mn Spinel Oxide Nanospheres Anchored N-Doped Carbon Activated Peroxymonosulfate. *Chem. Eng. J.* **2024**, *497*, 154687. https://doi.org/10.1016/j.cej.2024.154687.

9. Wang, X.; Zhuang, Y.; Zhang, J.; Song, L.; Shi, B. Pollutant Degradation Behaviors in a Heterogeneous Fenton System through Fe/S-Doped Aerogel. *Science of The Total Environment* **2020**, *714*, 136436. https://doi.org/10.1016/j.scitotenv.2019.136436.
10. Zhang, S.; Wu, D. Activation of Peroxymonosulfate by FeOOH Modified Biochar for the Degradation of Tetracycline Hydrochloride. *Materials Letters* **2024**, *375*, 137218. https://doi.org/10.1016/j.matlet.2024.137218.
11. Zhang, G.; Xia, S.; Li, H.; Du, H.; Li, T.; Cao, Y.; Meng, Y.; Wang, J.; Zhong, C.; Lau, W.-M. Mediated Peroxydisulfate Activation at Oxygen Vacancy Sites: Synergistic Degradation of Norfloxacin by Radical Pathway and Non-Radical Pathway. *Separation and Purification Technology* **2025**, *354*, 129018. https://doi.org/10.1016/j.seppur.2024.129018.
12. Sun, H.; Kwan, C.; Suvorova, A.; Ang, H. M.; Tadé, M. O.; Wang, S. Catalytic Oxidation of Organic Pollutants on Pristine and Surface Nitrogen-Modified Carbon Nanotubes with Sulfate Radicals. *Applied Catalysis B: Environmental* **2014**, *154–155*, 134–141. https://doi.org/10.1016/j.apcatb.2014.02.012.
13. Cao, J.; Sun, S.; Li, X.; Yang, Z.; Xiong, W.; Wu, Y.; Jia, M.; Zhou, Y.; Zhou, C.; Zhang, Y. Efficient Charge Transfer in Aluminum-Cobalt Layered Double Hydroxide Derived from Co-ZIF for Enhanced Catalytic Degradation of Tetracycline through Peroxymonosulfate Activation. *Chemical Engineering Journal* **2020**, *382*, 122802. https://doi.org/10.1016/j.cej.2019.122802.
14. Li, Y.; Pan, L.; Zhu, Y.; Yu, Y.; Wang, D.; Yang, G.; Yuan, X.; Liu, X.; Li, H.; Zhang, J. How Does Zero Valent Iron Activating Peroxydisulfate Improve the Dewatering of Anaerobically Digested Sludge? *Water Res.* **2019**, *163*, 114912. https://doi.org/10.1016/j.watres.2019.114912.
15. Asif, B. M.; Ji, B.; Maqbool, T.; Zhang, Z. Algogenic Organic Matter Fouling Alleviation in Membrane Distillation by Peroxymonosulfate (PMS): Role of PMS Concentration and Activation Temperature. *Desalination* **2021**, *516*, 115225. https://doi.org/10.1016/j.desal.2021.115225.
16. Khataee, A. Application of Central Composite Design for the Optimization of Photo-Destruction of a Textile Dye Using UV/SO Process. *Polish Journal of Chemical Technology* **2009**, *11* (4), 38–45. https://doi.org/10.2478/v10026-009-0041-y.
17. Li, H.; Wan, J.; Ma, Y.; Huang, M.; Wang, Y.; Chen, Y. New Insights into the Role of Zero-Valent Iron Surface Oxidation Layers in Persulfate Oxidation of Dibutyl Phthalate Solutions. *Chemical Engineering Journal* **2014**, *250*, 137–147. https://doi.org/10.1016/j.cej.2014.03.092.
18. Qian, Y.; Zhang, F.; Pang, H. A Review of MOFs and Their Composites-Based Photocatalysts: Synthesis and Applications. *Advanced Functional Materials* **2021**, *31* (37), 2104231. https://doi.org/10.1002/adfm.202104231.
19. Du, X.; Zhou, M. Strategies to Enhance Catalytic Performance of Metal–Organic Frameworks in Sulfate Radical-Based Advanced Oxidation Processes for Organic Pollutants Removal. *Chemical Engineering Journal* **2021**, *403*, 126346. https://doi.org/10.1016/j.cej.2020.126346.
20. Li, Z.; Tang, X.; Huang, G.; Luo, X.; He, D.; Peng, Q.; Huang, J.; Ao, M.; Liu, K. Bismuth MOFs Based Hierarchical Co_3O_4-Bi_2O_3 Composite: An Efficient Heterogeneous Peroxymonosulfate Activator for Azo Dyes Degradation. *Separation and Purification Technology* **2020**, *242*, 116825. https://doi.org/10.1016/j.seppur.2020.116825.
21. Guo, H.; Zhang, J.; Yang, F.; Wang, M.; Zhang, T.; Hao, Y.; Yang, W. Sandwich-like Porous MXene/Ni_3S_4/CuS Derived from MOFs as Superior Supercapacitor Electrode. *Journal of Alloys and Compounds* **2022**, *906*, 163863. https://doi.org/10.1016/j.jallcom.2022.163863.
22. Wang, R.; Dong, X.-Y.; Du, J.; Zhao, J.-Y.; Zang, S.-Q. MOF-Derived Bifunctional Cu_3P Nanoparticles Coated by a N,P-Codoped Carbon Shell for Hydrogen Evolution and Oxygen Reduction. *Advanced Materials* **2018**, *30* (6), 1703711. https://doi.org/10.1002/adma.201703711.
23. Behera, P.; Subudhi, S.; Tripathy, S. P.; Parida, K. MOF Derived Nano-Materials: A Recent Progress in Strategic Fabrication, Characterization and Mechanistic Insight towards Divergent Photocatalytic Applications. *Coordination Chemistry Reviews* **2022**, *456*, 214392. https://doi.org/10.1016/j.ccr.2021.214392.
24. Liu, D.; Gu, W.; Zhou, L.; Wang, L.; Zhang, J.; Liu, Y.; Lei, J. Recent Advances in MOF-Derived Carbon-Based Nanomaterials for Environmental Applications in Adsorption and Catalytic Degradation. *Chemical Engineering Journal* **2022**, *427*, 131503. https://doi.org/10.1016/j.cej.2021.131503.
25. Cheng, Y.; Hao, Z.; Hao, C.; Deng, Y.; Li, X.; Li, K.; Zhao, Y. A Review of Modification of Carbon Electrode Material in Capacitive Deionization. *RSC Adv.* **2019**, *9* (42), 24401–24419. https://doi.org/10.1039/C9RA04426D.
26. Yu, X.; Wang, L.; Shen, X.; Wu, Y.; Xu, L.; Zhang, Y.; Shi, J.; Gan, L. New Insight into the S and N Co-Doped Poplar Biochar for Efficient BPA Removal via Peroxymonosulfate Activation: S for Adsorptive Removal and N for Catalytic Removal. *Separation and Purification Technology* **2025**, *354*, 128809. https://doi.org/10.1016/j.seppur.2024.128809.
27. He, Y.; Yang, Y.; Ye, X.; Lv, Y.; Liu, Y.; Liu, M. Enhanced Persulfate Activation for Sulfadiazine Degradation by N, S Self-Doped Biochar from Sludge and Sulfonated Lignin: Emphasizing the Roles of Graphitic Nitrogen and Thiophene Sulfur. *Journal of Environmental Chemical Engineering* **2024**, *12* (3), 112407. https://doi.org/10.1016/j.jece.2024.112407.

28. Qu, G.; Jia, P.; Zhang, T.; Tang, S.; Pervez, Md. N.; Pang, Y.; Li, B.; Cao, C.; Zhao, Y. Synergistic Activation of Peroxymonosulfate by Intrinsic Defect and Graphitic N of N, P Co-Doped Carbon Microspheres for BPA Degradation. *Chem. Eng. J.* **2023**, *475*, 145888. https://doi.org/10.1016/j.cej.2023.145888.
29. Chen, W.; Lei, L.; Zhu, K.; He, D.; He, H.; Li, X.; Wang, Y.; Huang, J.; Ai, Y. Peroxymonosulfate Activation by Fe-N-S Co-Doped Tremella-like Carbocatalyst for Degradation of Bisphenol A: Synergistic Effect of Pyridine N, Fe-Nx, Thiophene S. *J. Environ. Sci.* **2023**, *129*, 213–228. https://doi.org/10.1016/j.jes.2022.09.037.
30. Ma, W.; Wang, N.; Tong, T.; Zhang, L.; Lin, K.-Y. A.; Han, X.; Du, Y. Nitrogen, Phosphorus, and Sulfur Tri-Doped Hollow Carbon Shells Derived from ZIF-67@poly (Cyclotriphosphazene-Co-4, 4′-Sulfonyldiphenol) as a Robust Catalyst of Peroxymonosulfate Activation for Degradation of Bisphenol A. *Carbon* **2018**, *137*, 291–303. https://doi.org/10.1016/j.carbon.2018.05.039.
31. Zhang, H.; Cui, H.; Li, J.; Liu, Y.; Yang, Y.; Wang, M. Frogspawn Inspired Hollow Fe_3C@N–C as an Efficient Sulfur Host for High-Rate Lithium–Sulfur Batteries. *Nanoscale* **2019**, *11* (44), 21532–21541. https://doi.org/10.1039/C9NR07388D.
32. Long, Y.; Bu, S.; Huang, Y.; Shao, Y.; Xiao, L.; Shi, X. N-Doped Hierarchically Porous Carbon for Highly Efficient Metal-Free Catalytic Activation of Peroxymonosulfate in Water: A Non-Radical Mechanism. *Chemosphere* **2019**, *216*, 545–555. https://doi.org/10.1016/j.chemosphere.2018.10.175.
33. Li, X.; Ye, L.; Ye, Z.; Xie, S.; Qiu, Y.; Liao, F.; Lin, C.; Liu, M. N, P Co-Doped Core/Shell Porous Carbon as a Highly Efficient Peroxymonosulfate Activator for Phenol Degradation. *Sep. Purif. Technol.* **2021**, *276*, 119286. https://doi.org/10.1016/j.seppur.2021.119286.
34. Lai, L.; Potts, J. R.; Zhan, D.; Wang, L.; Poh, C. K.; Tang, C.; Gong, H.; Shen, Z.; Lin, J.; Ruoff, R. S. Exploration of the Active Center Structure of Nitrogen-Doped Graphene-Based Catalysts for Oxygen Reduction Reaction. *Energy Environ. Sci.* **2012**, *5* (7), 7936–7942. https://doi.org/10.1039/C2EE21802J.
35. Wang, C.; Kim, J.; Kim, M.; Lim, H.; Zhang, M.; You, J.; Yun, J.-H.; Bando, Y.; Li, J.; Yamauchi, Y. Nanoarchitectured Metal–Organic Framework-Derived Hollow Carbon Nanofiber Filters for Advanced Oxidation Processes. *J. Mater. Chem.a* **2019**, *7* (22), 13743–13750. https://doi.org/10.1039/C9TA03128F.
36. Cui, Q.; Zhang, W.; Chai, S.; Zuo, Q.; Kim, K.-H. The Potential of Green Biochar Generated from Biogas Residue as a Heterogeneous Persulfate Activator and Its Non-Radical Degradation Pathways: Adsorption and Degradation of Tetracycline. *Environ. Res.* **2022**, *204*, 112335. https://doi.org/10.1016/j.envres.2021.112335.
37. Oh, W.-D.; Dong, Z.; Lim, T.-T. Generation of Sulfate Radical through Heterogeneous Catalysis for Organic Contaminants Removal: Current Development, Challenges and Prospects. *Appl. Catal. B* **2016**, *194*, 169–201. https://doi.org/10.1016/j.apcatb.2016.04.003.
38. Yin, R.; Guo, W.; Wang, H.; Du, J.; Wu, Q.; Chang, J.-S.; Ren, N. Singlet Oxygen-Dominated Peroxydisulfate Activation by Sludge-Derived Biochar for Sulfamethoxazole Degradation through a Nonradical Oxidation Pathway: Performance and Mechanism. *Chem. Eng. J.* **2019**, *357*, 589–599. https://doi.org/10.1016/j.cej.2018.09.184.
39. Zhang, W.; Liu, J.; Tan, J.; Yu, H.; Liu, X. Facile Route for Fabricating $Co(OH)_2$@WO_3 Microspheres from Scheelite and Its Environmental Application for High-Performance Peroxymonosulfate Activation. *J. Cleaner Prod.* **2022**, *340*, 130714. https://doi.org/10.1016/j.jclepro.2022.130714.
40. Gu, A.; Wang, P.; Chen, K.; Djam Miensah, E.; Gong, C.; Jiao, Y.; Mao, P.; Chen, K.; Jiang, J.; Liu, Y.; Yang, Y. Core-Shell Bimetallic Fe-Co MOFs to Activated Peroxymonosulfate for Efficient Degradation of 2-Chlorophenol. *Sep. Purif. Technol.* **2022**, *298*, 121461. https://doi.org/10.1016/j.seppur.2022.121461.
41. Hu, P.; Su, H.; Chen, Z.; Yu, C.; Li, Q.; Zhou, B.; Alvarez, P. J. J.; Long, M. Selective Degradation of Organic Pollutants Using an Efficient Metal-Free Catalyst Derived from Carbonized Polypyrrole via Peroxymonosulfate Activation. *Environ. Sci. Technol.* **2017**, *51* (19), 11288–11296. https://doi.org/10.1021/acs.est.7b03014.
42. Gong, C.; Chen, F.; Yang, Q.; Luo, K.; Yao, F.; Wang, S.; Wang, X.; Wu, J.; Li, X.; Wang, D.; Zeng, G. Heterogeneous Activation of Peroxymonosulfate by Fe-Co Layered Doubled Hydroxide for Efficient Catalytic Degradation of Rhoadmine B. *Chem. Eng. J.* **2017**, *321*, 222–232. https://doi.org/10.1016/j.cej.2017.03.117.
43. Liu, F.; Cao, J.; Yang, Z.; Xiong, W.; Xu, Z.; Song, P.; Jia, M.; Sun, S.; Zhang, Y.; Zhong, X. Heterogeneous Activation of Peroxymonosulfate by Cobalt-Doped MIL-53(Al) for Efficient Tetracycline Degradation in Water: Coexistence of Radical and Non-Radical Reactions. *J. Colloid Interface Sci.* **2021**, *581*, 195–204. https://doi.org/10.1016/j.jcis.2020.07.100.